Geometry and thermal regime of the southern outlet glaciers of Qaanaaq Ice Cap, NW Greenland

Lamsters, K., [a], Karušs, J.,[a] Ješkins, J., [a] Džeriņš, P. [a], Ukai, S. [b], Sugiyama, S. [b]

[a] – Faculty of Geography and Earth Sciences, University of Latvia, Jelgavas street 1, Riga, LV-1004, Latvia.
[b]– Institute of Low Temperature Science, Hokkaido University, Nishi 8, Kita 19, Sapporo, 060-0819, Japan.

e-mails:
Kristaps Lamsters: kristaps.lamsters@lu.lv
Jānis Karušs: janis.karuss@lu.lv
Jurijs Ješkins: jurijs.jeskins@lu.lv
Pēteris Džeriņš: peteris.dzerins@lu.lv
Shin Sugiyama: sugishin@lowtem.hokudai.ac.jp
Shinta Ukai: ukaishinta@ees.hokudai.ac.jp

Abstract
Glaciers and ice caps surrounding the Greenland Ice Sheet are found to be sensitive to warming climate thus the knowledge of their thickness and internal structure is substantial to determine their future impact on sea level and local environment. Still, in-situ glaciological measurements of such glaciers are very scarce. Here, we present the results of ground penetrating radar (GPR) and uncrewed aerial vehicle surveys conducted on the two southern outlet glaciers of Qaanaaq Ice Cap in NW Greenland. GPR measurements reveal up to 170 m thick ice and the lack of englacial hyperbolae indicating no developed en/subglacial drainage system. The glaciers consist mainly of radar transparent facies characteristic for cold ice, while limited scattering facies appear closer to the glacier's terminus beneath the thinnest ice and are attributed to debris inside the ice. Results

show that the glaciers flow into narrow V-shaped valleys suggesting spatio-temporally limited subglacial erosion and restricted possible distribution of temperate ice in the past. The comparison of the ice thickness measurement data with global ice thickness model estimates shows considerable discrepancies emphasising the need of modelling improvements in the case of narrow valley and outlet glaciers.

Keywords: unmanned aerial vehicle, glacier thermal structure, V-shaped valley, Greenland, ground penetrating radar.

1. INTRODUCTION

The retreat rate of peripheral glaciers and ice caps (GICs) in Greenland has doubled in the 21st century comparing with the 20th century (Larocca et al., 2023). The mass balance has become even three times more negative in glacier ablation areas (Carrivick et al., 2023). Increased mass loss of the GICs related with a rise in air temperatures has already been observed in the recent decades in NW Greenland (Saito et al., 2016; Khan et al., 2022). As the Arctic continues to warm at a greater rate than the global average (IPCC, 2021), glaciers in Greenland are receding more rapidly producing increased runoff and affecting marine ecosystems and local communities (Sugiyama et al., 2021).

In contrast to intensive research on the Greenland Ice Sheet (GrIS), studies on GICs in Greenland are relatively sparse despite their sensitivity and relatively short response time to climate change (Khan et al., 2022), governed by their location at lower elevations and proximity to the coast (Saito et al., 2016). As field investigations on GICs are sparse in Greenland, currently available data rely mainly on satellite remote sensing and may lack temporal and spatial resolution required for detailed studies.

Studies show that the rate of the mass loss of peripheral glaciers is not uniformly distributed along the coast of Greenland (Bolch et al., 2013; Khan et al., 2022) suggesting variable glacier changes as a response to regionally variable climate change and other local factors (Carrivick et al., 2023). Only detailed in-situ measurements may provide the quantification and monitoring of such glacier geometries, thermal structures and drainage systems. Such data for peripheral glaciers and ice caps around Greenland are very scarce, for example, the terrestrial ice thickness measurements by ground penetrating radar (GPR) were done for only eight glaciers as mentioned by Gillespie et al. (2023).

Commonly, in-situ ice thickness and thermal structure of a glacier is investigated by GPR surveys (e.g. Björnsson et al., 1996; Bælum & Benn, 2011; Irvine-Fynn et al., 2011; Rippin et al., 2011; Sevestre et al., 2015; Karušs et al., 2019; 2022a; 2022b; Lamsters et al., 2020a, 2020b). The possible polythermal structure of High Arctic glaciers is complex and difficult to reproduce by numerical simulations as studies show great differences between numerical modelling and in situ observations (e.g. Tsutaki et al., 2017). The highly variable thermal structure of Arctic glaciers is shown in numerous studies (e.g. Björnsson et al., 1996; Irvine-Fynn et al., 2011). The thermal structure of such glaciers is often not in a phase with a current warming climate usually leading to changes from polythermal structure to even entirely cold (Rippin et al., 2011; Sevestre et al., 2015; Karušs et al., 2022a, 2022b; Carrivick et al., 2023). The glacier thermal structure is related to and dependent on many factors including ice thickness, snow and firn layer thickness, presence of crevasses, surface meltwater percolation and freezing leading to cryo-hydrological warming, glacier geometry and dynamics including ice flow velocity, englacial strain distribution and frictional heating, and glacier history (e.g. Murray et al., 2000; Irvine-Fynn et al., 2011; Rippin et al., 2011; Forte et al., 2021; Karušs et al., 2022a; 2022b; Carrivick et al., 2023; Gillespie et al., 2023). The role of ice thickness in a glacier thermal structure is has occasionally been simplified and considered as superior leading, for example, to an assumption that there exists an ice thickness threshold of ~80–100 m, which is enough to sustain temperate ice (Hagen et al., 1993; Murray et al., 2000; Carrivick et al., 2023). Measurement data (e.g. Rippin et al., 2011; Forte et al., 2021; Karušs et al., 2022a, 2022b; Gillespie et al., 2023), however, show that temperate ice occasionally exists beneath thinner ice as a remnant of previous conditions or due to cryo-hydrological warming effect. The ice thickness, thermal structure and meltwater availability at the glacier bed are also one of the main factors influencing subglacial erosion usually leading to the formation of U-shaped valleys (Montgomery, 2002; Zimmer & Gabet, 2018), which may not be always the case for small and cold glaciers (e.g. Bælum & Benn, 2011).

Qaanaaq Ice Cap (QIC) and its outlet glaciers have been studied by the Japanese research groups (e.g. Sugiyama et al., 2014; Saito et al., 2016; Tsutaki et al., 2017; Sugiyama, 2020). However, ice thickness up to now has been measured only for the Qaanaaq Glacier (QG) and only pointwise along the one longitudinal survey route with 200 m interval in 2012 (Sugiyama et al., 2014). No other ice thickness or thermal structure surveys of the QIC have been published except of global modelling results (e.g. Millan et al., 2022). These modelling data of glacier thickness (e.g. Millan et al., 2022) has also allowed the reconstruction of the ice thickness and glacier thermal structure in the past (Carrivick et al., 2023), but such data computed for small high Arctic glacier requires validation.

Up to date, sufficiently reliable and detailed glaciological information on thickness, bed topography, thermal structure, and englacial/subglacial drainage is lacking at the QIC. Therefore, in this study, we aimed to obtain new detailed data of the QG and nearby unnamed glacier (UnG) of key glaciological parameters to characterize glacier geometry, ice thickness and glacier bed elevation variations together with data on ice thermal structure using GPR, Uncrewed Aerial Vehicle (UAV) surveys and global navigation satellite system (GNSS) measurements.

2. STUDY AREA

Our study area – QIC, is located at the Piulip Nunaa peninsula in Thule region of NW Kalaallit Nunaat, NW Greenland. It covers an area of approximately 260 km^2 and reaches the altitude of ~1100 m a.s.l. Our study site includes the QG and UnG situated 3 km from Qaanaaq village in the southern part of the QIC (Figure 1). These glaciers flow into narrow valleys, which are carved mainly in Mesoproterozoic sedimentary rocks (siltstones to conglomerates) (Carrivick et al., 2023) overlying Archean gneiss (Henriksen et al., 2009). Steep valley slopes with bedded sandstones are occasionally visible in proglacial areas (Figure 2a, c).

The first glaciological measurements and observations of the QG started in 2012 (Sugiyama et al., 2014; Kondo et al., 2021). The reconstructed glacial history of the QIC suggests that it survived the Holocene Thermal Maximum but was smaller than present at least from 3.3 ± 0.1 ka to 0.9 ± 0.1 ka cal a BP and before advance during the Neoglacial, especially the Little Ice Age. (Søndergaarde et., 2019; Carrivick et al., 2023). Specifically, 14C dating of subfossil plants near the southern ice margin of the QIC and the QG suggests that at around 3.1-3.3 ka moss were growing there, thus until that time the QIS was smaller than present, and glacier advance beyond the modern-day position occurred only later (Søndergaarde et., 2019).

The mean annual air temperature at Qaanaaq Airport (16 m a.s.l.) as reported by Tsutaki et al. (2017) from 2005 to 2015 was -8.5°C. The ice-cap-wide mass balance of the QIC from 2012 to 2016 was negative (-0.49 ±0.27 m w.e. a-1), although fluctuating substantially from -1.10 ± 0.29 in 2014/15 to -0.13 ± 0.26 m w.e. a-1 in 2012/13 (ibid.). Mass balance for the same period for the QG ranged from -2.15 ± 0.07 to -0.09 ± 0.03 m w.e. a-1. Annual ice flow velocities reached up to 20 m a-1 in the thickest part of the glacier at 584 m a.s.l. The maximum mean summer ice flow rate was 25 m a-1 at 740 m a.s.l. for 2012 (ibid.). A seasonal ice velocity speedup of the QG was recorded in 2012 by Tsutaki et al. (2017) who also suggested that an extraordinary amount of meltwater should have penetrated to the glacier bed in order to enhance rapid basal ice motion. However, such events are not typical, and it was connected to extreme melt across the GrIS in 2012 (Nghiem et al., 2012; Tsutaki et al., 2017). The mean equilibrium line altitude of the QG was 910 m a.s.l. for 2012–2016 (ibid.).

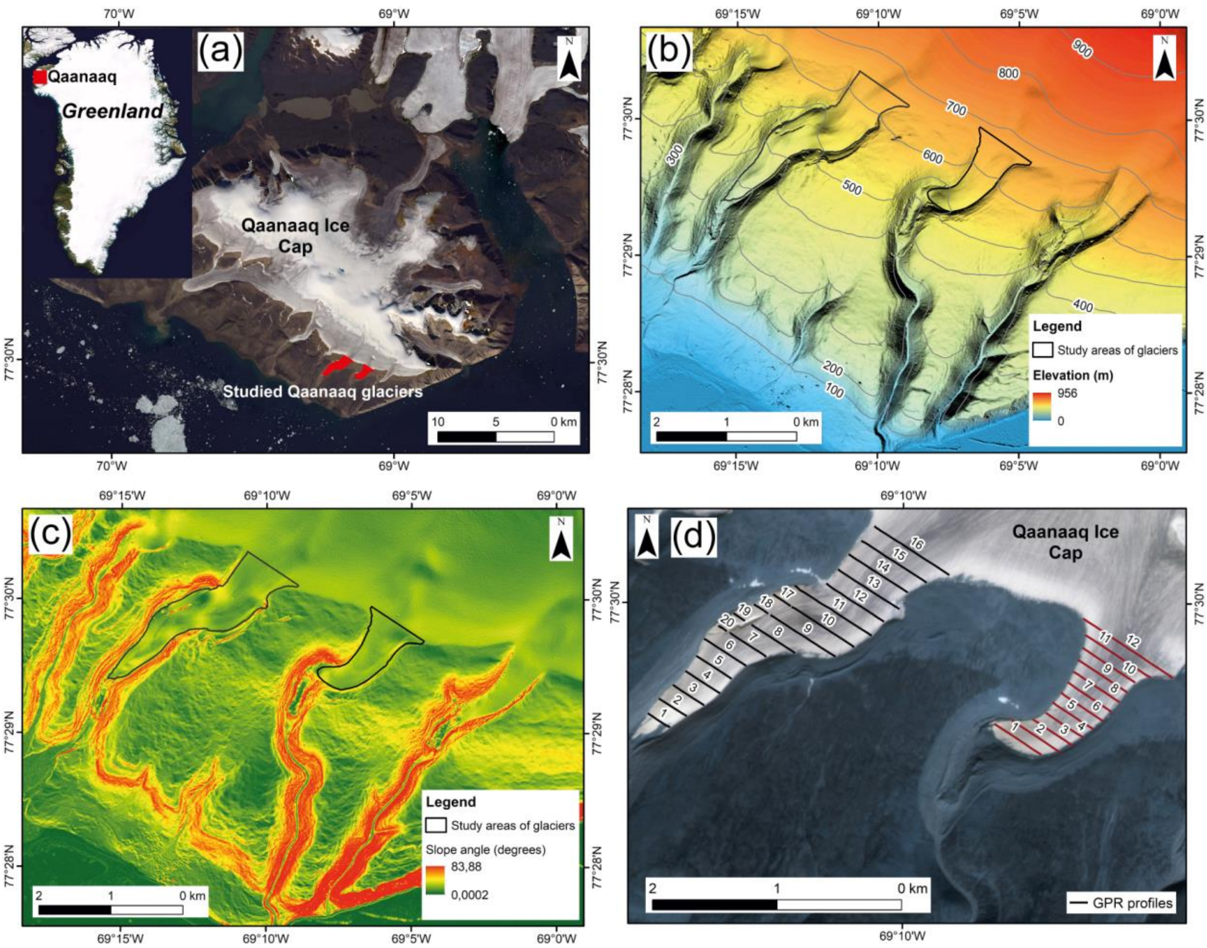

Figure 1. Location of studied glaciers and GPR profiles. (a) Satellite image of Greenland and QIC. Background: Natural-colour image of USGS Landsat 8 Level 2, Collection 2, Tier 1, August 2022. (b) ArcticDEM of studied glaciers and surroundings (Porter et al., 2023). (c) Slope of studied glaciers and surroundings from ArcticDEM. (d) Location of GPR profiles. Background: 3-m-resolution PlanetScope satellite image, August 2022.

Figure 2. Photos from the field. (a) A view towards the QIC and QG. Note the steep valleys. (b) GPR equipment and operator near a deep supraglacial stream valley. Note visible glacier internal layering. (c) A view from the QIC where the UnG flows into the sinuous V-shaped valley. (d) Transverse sediment accumulations melting from the snout of the QIC. Note also transverse ridges in front of the ice margin.

3. METHODS

Field surveys were conducted from August 1 to 12, 2022, on two glaciers of the QIC – the QG and UnG to the southeast (Figures 1-2). Ice thickness and internal structure of the glaciers was studied using GPR, while UAV surveys allowed to obtain the orthophoto and a detailed digital elevation model (DEM) of the QG with a resolution of 92 mm. For the studied areas, the ice thickness and subglacial topography models were created. The UnG was surveyed only by GPR and GNSS.

3.1 GPR and GNSS surveys

A GPR survey was conducted using a Zond-12e double-channel GPR system equipped with 38 MHz (nominal frequency in the air) antenna (Figure 2b). We choose the antenna with the lowest frequency that is compatible with the Zond GPR system to ensure maximum possible signal penetration depth. Bandwidth at half of the received signal spectrum amplitude was 28 MHz (from 26 MHz to 54 MHz). The maximum time window of 2000 ns was used to allow the signal penetration up to the expected glacier bed. Spacing between the individual GPR traces was approximately 2 cm. To maintain regular grid of GPR profiles, a way-point plan was created before the survey adding at least one point after each 50 m. The walking velocity of the GPR operator was approximately constant for each 50 m. GPR profiles were oriented mainly transverse to the ice flow direction in order to ease data gathering and to better map the subglacial valley and possible englacial conduit system supposed to be almost perpendicular to the GPR profiles direction (Karušs et al., 2022b). The distance between transverse profiles was set to 150 m on the QG and 100 m on the UnG (Figure 1d).

GNSS receivers, Emlid RS2+, were employed for acquiring coordinates of the GPR profiles with ~50 m step. GNSS data collection was set up as follows: each point was measured for 20 seconds at a 5Hz update rate, yielding 100 measurements per point. The post-processing kinematics (PPK) method facilitated GPS coordinate acquisition. A GNSS base station was established near the polar base on each day of the GPR survey. The base station's log file recorded data throughout the day. Subsequently, these log files underwent processing using the NRCAN precise point positioning (PPP) service (Precise Point Positioning, n.d.) to obtain accurate coordinates. Log files were collected and processed accordingly. All survey points were converted to the WGS 84/UTM zone 19N coordinate system. These survey points were subsequently utilized for GPR data processing. The RMSE values of post-PPP processed base station coordinates were 0.32 cm for the X and Y axes and 0.39 cm for the Z-axis. For the PPK survey on the glaciers, the lateral and elevation RMSE values were less than 2 cm. All points were deemed reliable and were incorporated into the GPR processing.

The GPR data were processed with Prism 2.61 software. A manually adjusted time-dependent signal gain function, background removal filter, Ormsby band-pass filter with a low frequency cut off at 13 MHz and a high frequency cut off at 66 MHz, and migration using with the common midpoint method (CMP) determined GPR signal propagation speed was applied to the obtained radargrams. For the GPR profiles obtained on QG topographical correction was performed using elevations from UAV-derived DEM. Due to an unfortunate crash of UAV during the survey of UnG, we were not able to obtain DEM for the UnG, thus topographical correction was performed using DEM generated only from GNSS measurement points along the GPR profiles.

During the GPR data interpretation, the two-way travel time for the basal reflections was determined for each recorded radargram along its whole length. The distance between individual travel time measurements was approximately 10 m. Obtained travel time values were exported to ESRI ArcMap 10.8.1 for further ice thickness calculation and interpolation.

The GPR signal propagation speed was determined using CMP that has been proven to be effective not only on glaciers but also in various types of sediments (Karušs et al., 2021). We choose position for the CMP measurement point using common offset radargrams. Location where glacier surface and bed were relatively smooth and glacier thickness did not exceed ~50 m, was chosen ensuring clear and strong reflection from the glacier bed. During the acquisition of the data, transmitter and receiver antenna was moved apart with respect to a central fixed position in a direction perpendicular to the glacier flow direction. Offset between transmitting and receiving antennas was incremented from 1 to 97 m with a constant increment equal to 1 m.

Errors of the calculated depth values were determined using the approach described by Navarro & Eisen (2009) (pp. 195–231). It was assumed that uncertainty of the determined time values was half of the wavelength of received reflections, which corresponds to 13 ns, while for the uncertainty of the GPR signal propagation speed according to (Jacob & Hermance, 2004), 2% error was taken as a typical mean for the value obtained with CMP method.

3.2 UAV surveys and generation of maps

A UAV survey was performed on August 10–11, 2022 with a DJI Phantom 4 Pro V2.0 drone using the DJI Terra software. The drone was operated over the lower reaches of the QG (230–750 m a.s.l.) and aerial photographs were taken during the automated missions. The overlap between the images was ~70% and 65% along and across the flight path, respectively. The resolution of the images was 2.4–7.7 mm per pixel, depending on the flight height above surface. We distributed 24 pieces of painted wooden plates on the glacier as ground controlling points (GCPs) and they were surveyed by a static positioning technique with dual frequency global positioning system (GPS) receivers (Leica Geosystems, GS 10) and the Leica Infinity software.

Approximately 2000 images acquired by the UAV flights were processed using software Agisoft Metashape 1.7.1 to obtain a DEM and orthomosaic. We followed workflow and parameters suggested by previous studies in High Arctic (Ewertowski et al., 2019b; Karušs et al., 2022a; Lamsters et al., 2022). A three-dimensional point cloud obtained by the Structure from Motion algorithm was interpolated to generate a DEM with a horizontal resolution of 92 mm. The root mean square error of the GCPs was 0.095 m. The accuracy of the DEM was also assessed using the 213 elevation points measured by GNSS receivers as the ending and starting points of GPR profiles on the glacier. The largest errors were with the points on the highest GPR line where two DEM were mosaicked together and near the glacier margins. The standard deviation of all measured points comparing with DEM elevation, however, was low – 0.19 m.

Final maps were processed and generated in ESRI ArcMap10.8.1 using WGS 84/UTM zone 19N coordinate system and ellipsoidal height. UAV-derived orthophoto mosaic and DEM was imported in ArcMap. Maps of aspect and slope were produced from DEM. For the analysis of unglaciated valleys and visualisation purposes we used the newest ArcticDEM strip (SETSM_s2s041_WV02_20220727_10300100D6871300_10300100D727E900_2m_lsf_seg1) downloaded from https://fridge.pgc.umn.edu/ (Porter et al., 2023). A natural-colour image of USGS Landsat 8 Level 2, Collection 2, Tier 1 (LC08_L2SP_033005_20220802_20220805_02_T1_SR) was also used for the visualisation of a larger area. Glacier outlines were delineated from UAV orthomosaic for the QG and from PlanetScope 3-m-resolution satellite image (20220809_162400_89_2464_3B_AnalyticMS_SR_harmonized) for the UnG.

Ice thickness and subglacial topography models were prepared as follows. The ice thickness was calculated for the imported GPR measurement points from the picked travel time values using GPR signal propagation speed of 165 m ms-1 (see details in the following section – GPR signal speed). We compared kriging and spline interpolation methods and as they produced similar results in interpolating data. Then we chose to use spline interpolator with optimized tension parameter to obtain a smooth surface, but with a good correspondence to the measurement points. Ice thickness and subglacial topography models were generated with 1-m-cell size. Interpolated ice thickness was compared with a model of Millan et al. (2022) for the discussion of ice thickness threshold and temperate ice. Surface slope and interpolated ice thickness were used to calculate driving (shear) stress by multiplying ice density (917 kg m-3), acceleration due to gravity (9.81 m s-2), ice thickness and sine of surface slope in degrees (see Van der Veen & Whillans, 1989 and Rippin et al., 2011). For the visualisation purposes and to avoid local surface features we applied focal statistics tool in ArcMap with circle neighbourhood type and radius of 25 cells on a 1-m-resolution driving stress raster.

4. RESULTS AND INTERPRETATION

4.1. GPR signal speed

A clear reflection from the glacier bed is evident in CMP radargram (Figure 3a). It was possible to identify reflection from the glacier bed on 80 recorded traces. It was calculated that the mean ε was equal to 3.30 (corresponding GPR signal propagation speed of 165 m ms^{-1}) with the corresponding squared correlation coefficient 0.999 (Figure 3b). Despite the high value of the squared correlation coefficient, we assume that value of GPR signal propagation speed is determined with 2% error as suggested by Barrett et al. (2007). The obtained value is slightly higher than typical value that is assumed for cold ice (ε ≈ 3.2) (Bradford & Harper, 2005; Gusmeroli et al., 2010; Farinotti et al., 2014). Nonetheless, it fits in the interval of ε values reported for cold ice taking into consideration error of calculated value.

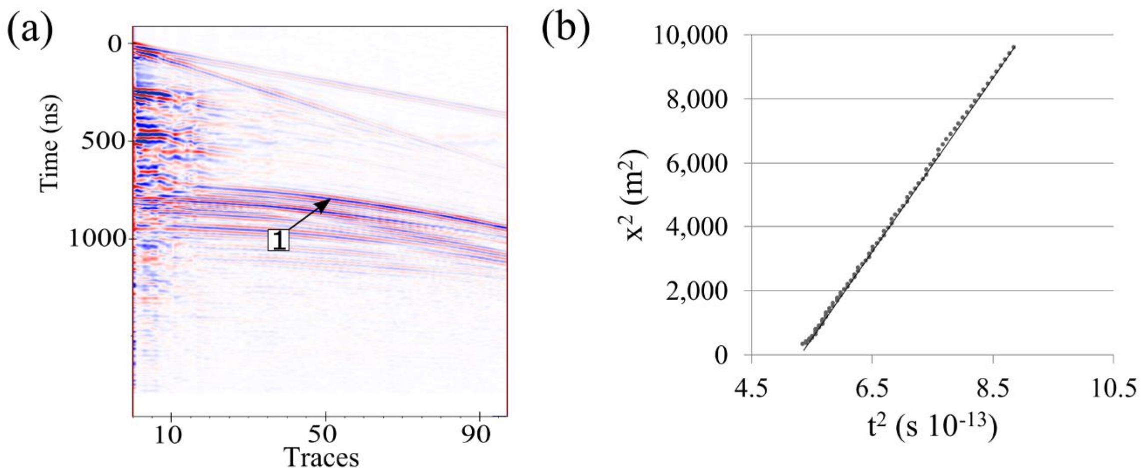

Figure 3. (a) A radargram obtained from the CMP measurements. (b) Constructed t^2x^2 graph. 1 – reflection form the bed of the glacier

4.2. Ice thickness and subglacial valley topography

GPR surveys were performed on 1.26 km^2 and 0.59 km^2 large areas of the QG and UnG, respectively, covering their full extent outside the ice cap (Figure 1d). The studied parts of the QG and the UnG are ~2.7 km and 1.5 km long respectively. The maximum measured ice thickness reaches 170.1 m for the QG and 129.4 m for the UnG. The average interpolated ice thickness is 62.9 m and 46.9 m, and the ice volume is 0.080 km^3 and 0.028 km^3 respectively. The uncertainty of glacier volumes may be similar to other studies (e.g. Yde et all., 2014) and account for up to ±10%.

Calculated depth uncertainty from the GPR measurement data near the glacier margins, where the ice is ~5 m deep, is ± 1.07 m, while at the highest part, where ice thickness is ~170 m, it reaches ± 3.2 m.

The areas with the greatest ice thickness of both studied glaciers occur along the central axis of the subglacial valleys (Figure 4e, Figure 5e). For the QG, the thickest ice occurs not in the upper reaches of the glacier but at 1.9 km from the glacier terminus and coincides with the broadest (at the valley bottom) and only part of the subglacial valley that may be considered as almost U-shaped. The rest of the subglacial valley of the QG and all subglacial valley of the UnG is very narrow and is clearly V-shaped (Figures 4f and 5b).

Except of the small, circular overdeeping in the middle of the glacier, the bed of the QG progressively decreases in the direction of the glacier terminus from ~490 m to ~225 m (here and after – above ellipsoid) along the central (deepest) axis of the subglacial valley. Maximum elevation differences of the glacier bed range from 640 m to 218 m, thus, the amplitude of the glacier bed altitude reaches 422 m. The subglacial valley is up to ~ 170 m deep at the highest end of the studied part of the glacier. Here, the glaciers fill the valley completely, thus this value may be considered as the maximum depth of this valley. The bed elevation of the UnG ranges from 400 to 665 m.

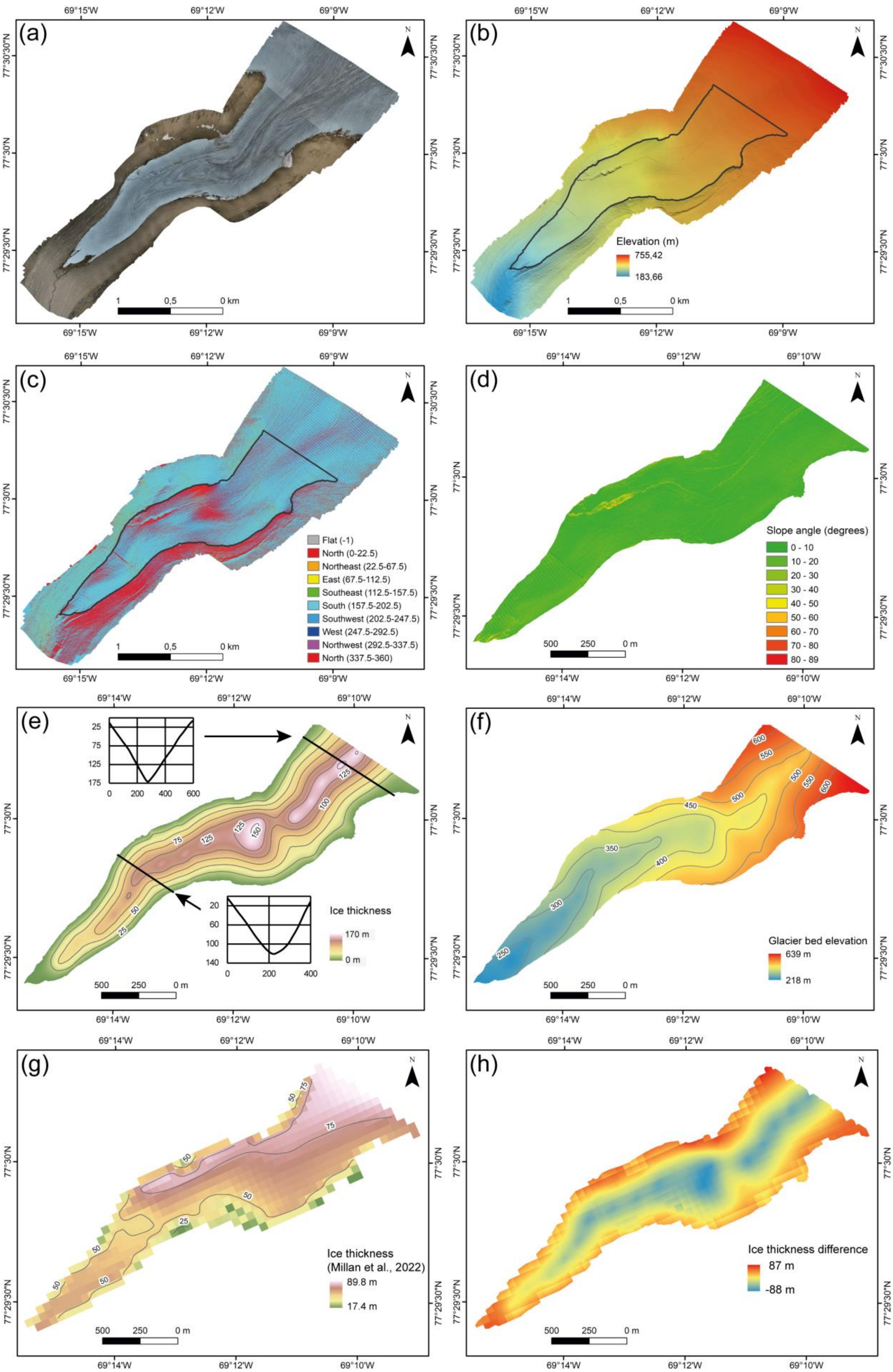
(a)
(b)
Elevation (m)
755,42
183,66
(c)
Flat (-1)
North (0-22.5)
Northeast (22.5-67.5)
East (67.5-112.5)
Southeast (112.5-157.5)
South (157.5-202.5)
Southwest (202.5-247.5)
West (247.5-292.5)
Northwest (292.5-337.5)
North (337.5-360)
(d)
Slope angle (degrees)
0 - 10
10 - 20
20 - 30
30 - 40
40 - 50
50 - 60
60 - 70
70 - 80
80 - 89
(e)
Ice thickness
170 m
0 m
(f)
Glacier bed elevation
639 m
218 m
(g)
Ice thickness
(Millan et al., 2022)
89.8 m
17.4 m
(h)
Ice thickness difference
87 m
-88 m
1 0,5 0 km
500 250 0 m
69°15'W
69°12'W
69°9'W
69°14'W
69°10'W
77°30'30"N
77°30'N
77°29'30"N

Figure 4. Generated maps and models of the QG: (a) UAV-derived orthomosaic; (b) UAV-derived DEM; (c) Aspect; (d) Slope; (e) Ice thickness, contours with 25 m increments; (f) Subglacial topography, contours with 50 m increments; (g) Ice thickness, contours with 25 m increments (Millan et al., 2022); (h) Ice thickness difference between this study and Millan et al. (2022). Note that in Figures 4a, b, c all UAV covered area is shown but, in the rest – only GPR covered part of the glacier.

Valley width to valley height (Vf) ratio as defined by formula of Bull & McFadden (1977), is less than 0.5 almost everywhere for the valley of the QG consistent with the visually obvious narrow V-shape valley type (calculated after ArcticDEM and subglacial topography obtained from GPR data). Only in a broader valley part beneath the thickest ice, it reaches little over 0.5. Subglacial valley of the UnG is quite similar and even narrower. As noted in the literature (Daxberger et al., 2014), Vf ratio values less than 1 indicate V-shaped valleys. The nearby small de-glaciated valleys in the southern part of the QIC are also mainly V-shaped.

The obtained UAV DEM and orthomosaic of the QG clearly reveals narrow valley slopes also outside the modern glacier limit. Closer to the glacier terminus, sedimentary rock outcrops are visible (Figures 2a and 4a) with defined trimlines of the LIA extent and are slightly scoured. The surface of the glacier is generally clean bare ice surface with supraglacial debris transport occurring only closely to the lateral margins. Frontal and lateral parts of the glacier surface are slightly covered with sediment drape indicating some englacial transport. There are many small supraglacial streams but only one deeply incised supraglacial channel fed by smaller ones up-glacier on each of the studied glaciers. This main channel does not reach the glacier terminus but flows to the lateral glacier margin and continues along the margin. In general, there is a lack of open crevasses (except of very small and shallow ones near lateral margins) and no moulins were detected on the studied parts of the glaciers, suggesting considerably limited surface meltwater penetration. Prominent transverse crevasses occur only in the higher elevation of the QIC outside of our study areas.

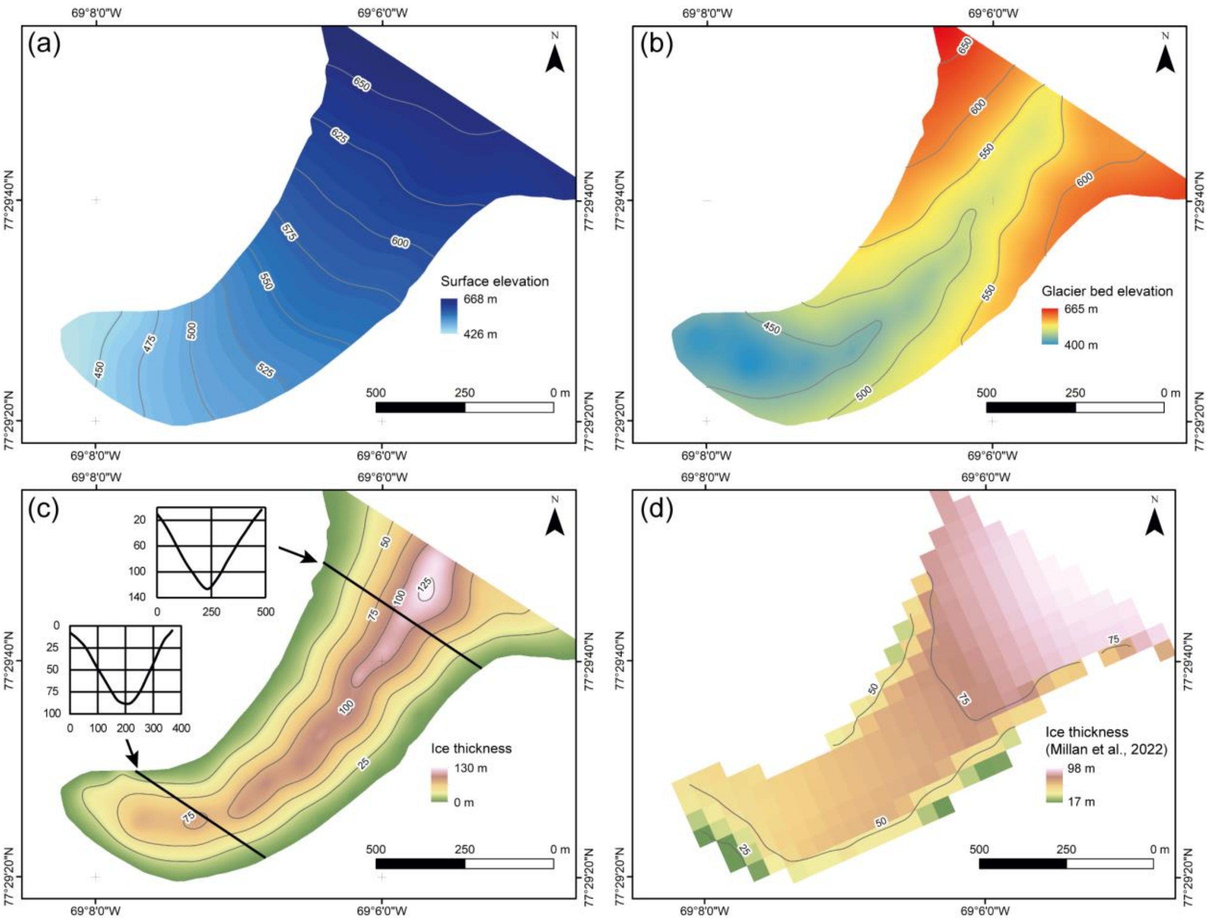

Figure 5. Generated maps and models of the UnG: (a) DEM; (b) Subglacial topography with contours after 50 m; (c) Ice thickness, contours with 25 m increments (this study); (d) Ice thickness, contours with 25 m increments (Millan et al., 2022).

The mean slope angle of the surface of the QG (from UAV-derived DEM), is 8.9 degrees (Figure 4d), while the angle of slope of subglacial valley for both studied glaciers is 24 degrees on average. Highest slope angles up to 89 degrees were reached in the main supraglacial channel. The slope and aspect maps of the QG (Figure 4c, d) allows also the more pronounced visualisation of surface structures attesting the lack of crevasses and emphasising surface drainage network.

The average calculated driving stress (81 kPa) is slightly lower than the values of 0.1 to 0.4 MPa usually mentioned in the literature (Brædstrup et al., 2016 and references therein). However, the highest stresses are up to 200 kPa (Figure 6) and coincide well with the areas of the largest ice thickness, located along the main axis of the subglacial valley. Very high stresses (up to 311 kPa) due to locally steep slopes occur also near the prominent supraglacial stream, which is deeply incised.

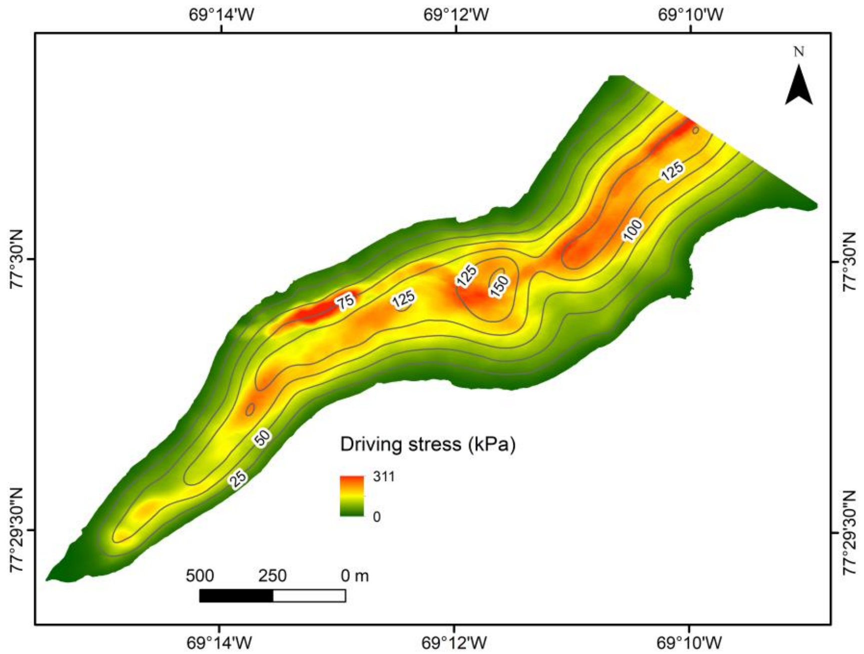

Figure 6. Driving stress across the QG in kPa. Black lines are contours of ice thickness for a comparison.

4.3. Thermal structure and englacial reflections

The studied glaciers consist mainly of radar transparent facies (Figures 7-8) and have strong basal reflections recording glacier bed. Inside the transparent radar facies, we found well-preserved internal layering. In the upper reaches of the studied glaciers, the layering is visible almost at the glacier bed and gradually decreases downglacier. This layering is only slightly deformed and mostly has concave appearance (Figures 7b, 8b) in accordance with valley topography suggesting converging ice flow into the subglacial valley and some internal deformation. Well-preserved internal layering also indicates restricted ice motion that may be characteristic for such a small, cold polar glaciers with also small erosion rates.

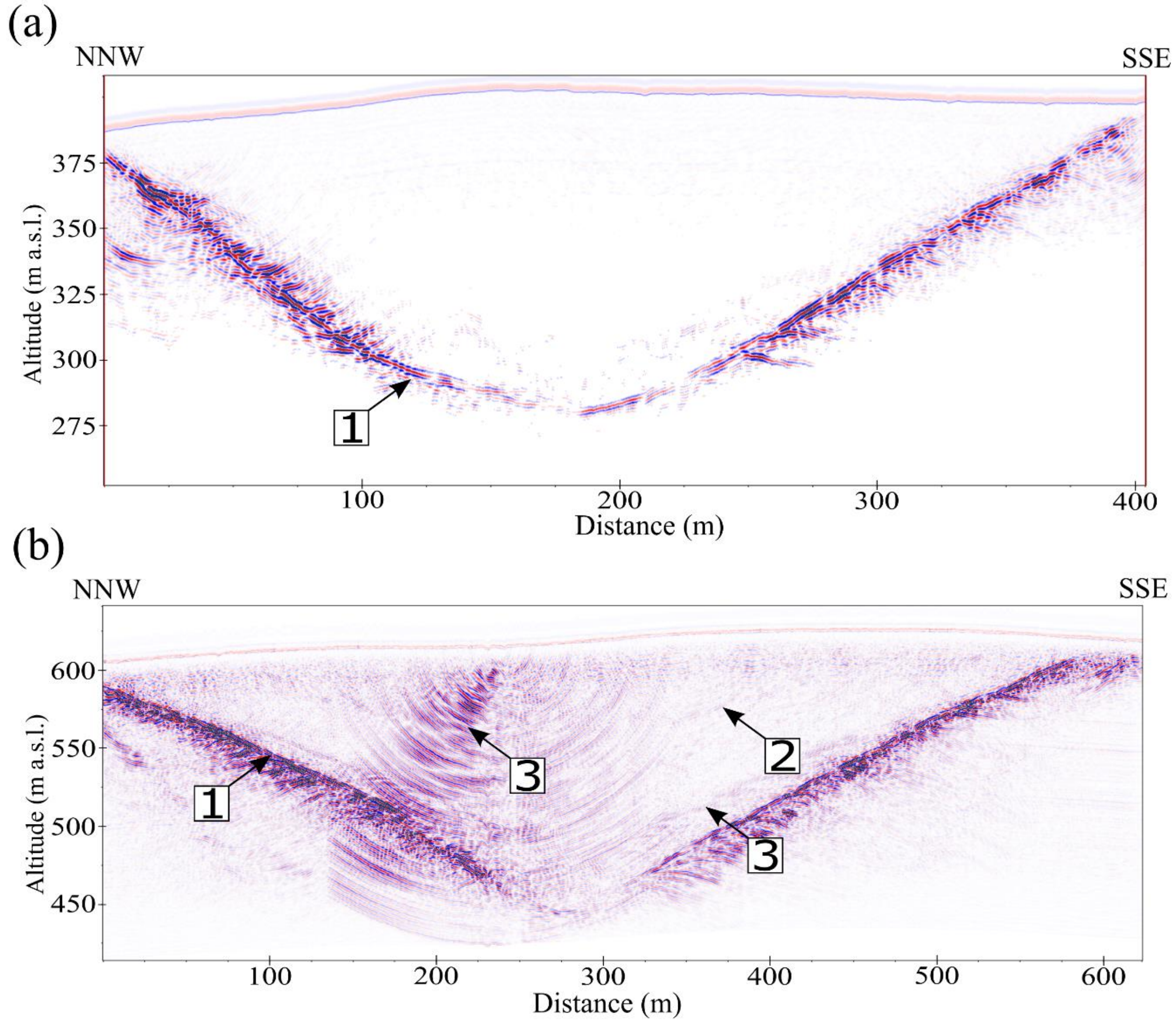

Figure 7. Examples of transverse GPR profiles on the QG: (a) Profile No. 6; (b) Profile No. 15. 1 – reflection related to the glacier bed. 2 – internal layering. 3 – migration artefact from supraglacial stream and bed of the glacier.

We also observe zones of intense scattering. The unevenly scattered signals in transverse GPR profiles occur mainly near the glaciers' terminus in the basal ice (Figures 7a and 8a). Near the glacier's terminus the scattering becomes more pronounced, and the thickness of high scattering zone increases despite the diminishing ice thickness. The maximum thickness of scattering facies is related to the thinnest ice as, for example, in the lowest GPR profile of the QG, where the maximum ice thickness is up to 50 m and scattering occurs almost near the glacier surface. In the next GPR profile, where the thickness is up to ~75 m, the scattering appears more than 30 m from the surface and is near the glacier bed in the next profile. The scattering is uneven with very undulating upper part and sometimes represented as stronger and weaker reflectors that show some inclination in transverse GPR profiles.

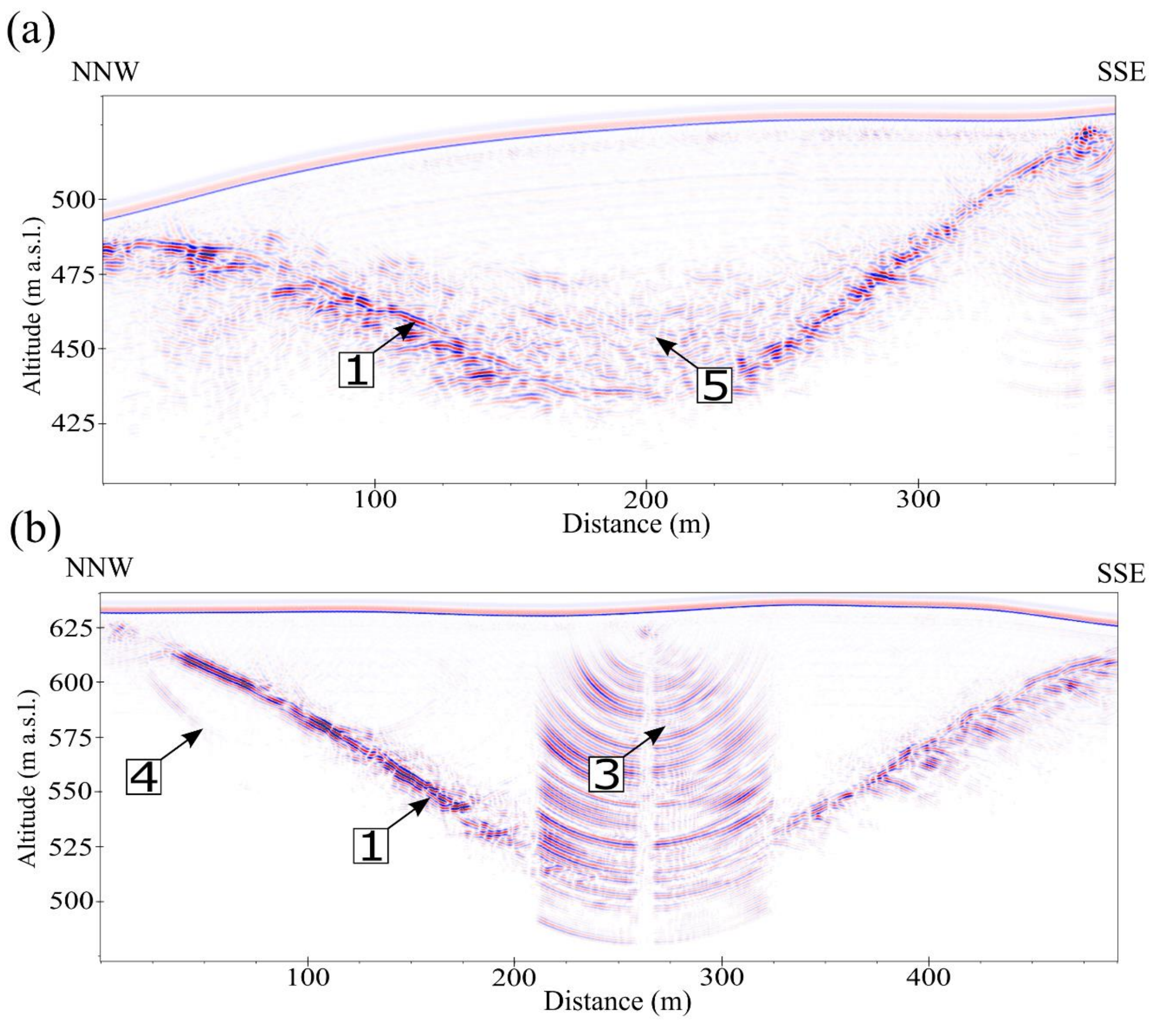

Figure 8. Examples of transverse GPR profiles on the UnG: (a) Profile No. 3. (b) Profile No. 10. 1 – reflection related to the glacier bed. 3 – migration

artefact from supraglacial stream. 4 – reflection from valley sidewall. 5 – reflections from debris within the ice.

Interpretation

Transparent facies are interpreted as cold ice according to common practice (Pettersson et al., 2003; Bælum & Benn, 2011; Karušs et al., 2022a; 2022b; Lamsters et al., 2020a; 2020b).

Scattering facies can be interpreted in different ways as temperate ice, water percolation zones, zones with dense crevasses, shear zones or debris rich ice (Björnsson et al., 1996; Pettersson et al., 2003; Sevestre et al., 2015; Lamsters et al., 2020a; 2020b; Forte et al., 2021; Karušs et al., 2022a; 2022 b; Santin et al., 2023). In our case, high scattering zones do not possess a distinct boundary with radar transparent facies as usually reported from polythermal glaciers where the cold/temperate ice transition is well-pronounced due to swift change in water content (e.g. Björnsson et al., 1996; Pettersson et al., 2003; Sevestre et al., 2015; Kauršs et al., 2022a;2022 b). Such an appearance of scattering is not typical for a scattering of temperate ice (see section 5.2. for further discussion) and together with a lack of meltwater penetration features allows to interpret it as debris inside the ice. Our interpretation is further supported by a presence of englacial debris melting out in the frontal part of the QIC and associated transverse ridges in the glacier forefield (Figure 2d), which most likely reveal the former positions of debris bands/thrust faults. Similar structures were observed and noted by Carrivick et al. (2023) from the QG, the UnG and several other glaciers of the QIC. There is geomorphologic evidence of cold-based ice margins of the studied glaciers as well, noted in this study, and by Carrivick et al. (2023) from the UnGs ush as an emergence of englacial debris with ice downwasting and burial of ice margins under coarse debris, thrusted sediments on the glacier surface, ice-cored moraines and sediment ridges associated with thrust planes, (Ewertowski et al., 2019a; Evans et al., 2022; Carrivick et al., 2023 and references therein).

An alternative interpretation of the scattering zones would relate them to temperate ice, but we do not favour this explanation due to low annual air temperatures and low ice thickness in this area (see more details in Discussion). Distinct diffraction hyperbolae are usually interpreted as crevasses, channels, or even large boulders or debris. In our case, there is a complete lack of hyperbolae inside the QG, which we interpret as a lack of englacial/subglacial channels. There are few hyperbolae present in the highest recorded GPR profile of the UnG. Due to their location close to the bedrock signal and the lateral margin of the glacier as well as the absence of the hyperbolae on following profiles, we interpret them as separate boulders that are detached from the glacier bed or debris concentrations. It is important that these hyperbolae are not only missing from the following GPR profiles but are rather represented as scattered signals near the glacier bed, which is also interpreted as debris inside the ice.

Subglacial and abandoned englacial conduits were observed by Carrivick et al. (2023) in the front of the Fan Glacier, which is also outlet glacier of the QIC, however, it is larger, much more dynamic and potentially a polythermal glacier comparing to the studied ones. The main supraglacial stream on each of the studied glaciers do not reach the frontal glacier margins but turns to the glacier lateral margins and flows along them. Distinct and vertically highly superimposed hyperbolae are visible in the upper GPR profiles (Figures 7b, 8b) of both glaciers where the main supraglacial stream exists. Open crevasses are largely missing from the glacier outlet parts (suggesting also low shear stresses). There is no proof for water reaching the glacier beds from GPR data, but this observation may be restricted to the studied part of the glaciers. Ice velocity measurements on the QIC showed diurnal and seasonal variations (Sugiyama et al., 2014; Tsutaki et al., 2017), which evinced water penetration to the bed during some summer melt seasons. Nevertheless, temporal velocity change was observed only in the upper reaches of the glacier above ~600 m a.s.l., suggesting restricted amount of meltwater and no impact on glacier velocity or thermal structure in the studied area.

5. DISCUSSION

In the following sub-section 5.1. we discuss our results in a relation with thermal structure and ice thickness of the Arctic glaciers and shortcomings of ice thickness model and reconstructions of past glacier thermal structure. In the sub-section 5.2. we analyse the subglacial topography of the studied glaciers and discuss the formation of V- and U-shaped glaciated valleys, subglacial erosion and mechanisms behind that.

5.1. Thermal structure and ice thickness

Glaciers in high Arctic have a variable thermal structure, and polythermal structure is common, for example, in Svalbard (Sevestre et al., 2015; Karušs et al., 2022a, 2022b). Glaciers in Greenland, including those measured in this study, could possibly have polythermal structure and temperate ice at the base, most likely as the remnant feature due to thicker and more dynamic ice in the past (Sugiyama et al., 2014; Carrivick et al., 2023). Temperate ice could even develop today due to latent heat release from freezing meltwater (cryo-hydrologic warming) in crevasses as it was found, for example, at the Lyngmarksbræen Ice Cap, West Greenland (Gillespie et al., 2023).

Carrivick et al. (2023) reconstructed the ice thickness of the QIC during the LIA and used a threshold of 90 m to infer potential areas of temperate ice during the LIA. Using this approximation, they showed that the largest glaciers of the QIC was temperate and even smaller ones like the QG and its neighbours had temperate ice along valley axes with thickest ice and at the accumulation zones during the LIA. They also showed that the largest outlet glaciers are almost completely temperate today as their ice thickness exceeds 90 m and the same is true for the accumulation zones of smaller glaciers including the QG. Our GRP measurement data clearly contradicts these assumptions regarding the smaller outlet glaciers like the QG and UnG where no temperate ice was found. Furthermore, we emphasize that these small outlet glaciers actually have much thicker ice than shown in the ice thickness model of Millan et al. (2022), which was used by Carrivick et al. (2023). Thus, if we use 90 m ice thickness threshold, then temperate ice even today should be present along the valley bottom of the QG beneath the thickest ice, but this is not the case.

We further compared our data with the recent ice thickness model by Millan et al. (2022) to evaluate such model performance in small outlet glaciers in High Arctic. The maximum difference of the ice thickness between model of Millan et al. (2022) and our measurements reaches 88 m. Along the central axis of the QG, the modelled thickness is greatly underestimated, while it is overestimated at similar degree near the lateral margins (Figures 4e, g, h and 5c, d). The similar deviations can be determined for the UnG. The maximum ice thickness reaches 170.1 for the QG and 129.4 m for the UnG in our data, while it is only 89.8 and 98.1 accordingly in Millan et al. (2022) model. Besides, as Millan et al. (2022 used data form 2017-2018, the modelled ice thickness should even be larger due to negative mass balance of the studied glaciers. The difference in glacier volume is 19.3% for the QG and 10% for the UnG. Highly variable ice thickness outcomes of models have been showed in previous studies (e.g. Farinotti et al., 2017, 2019, Hock et al., 2019, 2023) as well suggesting the need to improve the input data and various algorithms and used constants. Our comparison suggests that also the latest generation models (e.g. Millan et al., 2022) need further improvements to accurately estimate the thickness of small and narrow valley glaciers where the ice thickness along the main axis of the valley is greatly underestimated.

The mentioned ice thickness threshold of 90 m by Carrivick et al. (2023) has been derived from earlier studies in Svalbard suggesting a threshold ice thickness of ~80–100 m which may be enough to sustain temperate ice (Hagen et al., 1993; Murray et al., 2000). This simplification was confirmed also in recent study at Waldemarbreen (Karušs et al., 2022b), however, the authors noted that temperate ice exists also in areas where the total ice thickness is as low as ~40 m in the accumulation area. The study at the neighbouring Irenebreen glacier (Karušs et al., 2022a) has revealed that the average ice thickness in its southern cirque where the temperate ice was distributed, equalled to 73 m possibly suggesting even lower ice thickness threshold. However, the authors (ibid.) also emphasised that the area of temperate ice coincides well with the most crevassed part of the glacier, suggesting that not only ice thickness has effect on temperate ice distribution there, but it may be related to cryo-hydrologic warming effect as well. Furthermore, two small areas with temperate ice were found locally near the southern lateral margin of the glacier but these were located almost at the glacier surface suggesting water percolation and/or possible cryo-hydrological warming (Karušs et al., 2022a) similarly to studies by Gillespie et al. (2023) in Greenland and Forte et al. (2021) in Central Alps. The above-mentioned emphasizes that there are several other factors besides the ice thickness that governs the distribution of temperate ice and even in the cases where the ice thickness is considered as the main factor, its threshold can be variable and thus misleading. Therefore, we suggest that such possible thresholds may be applied only at defined regions and for specific glacier types and climatic conditions, which remains to be determined in further investigations.

5.2. Valley morphology, subglacial erosion and generation of debris

U-shaped valleys are widely considered as characteristic features of glacial erosion resulting mainly form subglacial quarrying that includes extensional fracturing (Leith et al., 2014), although the exact process and controlling factors are complex and depend on many conditions including variations of bedrock composition, glacial dynamics and history. Strong differences in the net result of valley excavation by fluvial and glacial erosion are found suggesting several times higher volume of removed rock in glaciated valleys, especially in these with large drainage areas (e.g. Hirano & Aniya, 1988; Harbor, 1992; Hallet et al., 1996; Montgomery, 2002; Alley et al., 2019). Central parts of cold-based ice sheets covering crystalline rocks has preserved relict morphologies (Kleman & Hättestrand, 1997; Patton et al., 2022) and low inferred glacial erosion rates (e.g. Lidmar-Bergström, 1997). On the contrary, glaciated valleys (troughs) are zones with higher erosion rates due to selective linear erosion (Hall et al., 2013). Considerable variations in erosion between polar and temperate valley glaciers are reported in literature, (e.g. Hallet et al., 1996; Hall al., 2013; Alley et al., 2019; Jansen et al., 2019; Patton et al., 2022). The climate, glacier dimensions, ice thickness, velocity, thermal structure and meltwater availability together with subglacial topography, glacier bed lithology, structure, tectonics and glaciation history may be the main factors controlling subglacial erosion (ibid.). Regarding the QG, ice velocity is currently low (Tsutaki et al. (2017) similarly to other High Arctic glaciers (Lamsters et al., 2022), however the sedimentary bedrock may be considered as readily erodible.

The glacier thermal structure and its evolution will play a substantial role in erosion due to very different rates between cold-based and warm-based glaciers (Hallet et al., 1996; Montgomery, 2002; Koppes et al., 2015). Erosion is strongly affected by the glacier thermal regime, which may even control erosion rates together with climate more than the extent of ice cover, ice flux or sliding speeds (Koppes et al., 2015). The differences in erosion rates of polar versus temperate glaciers are also specifically controlled by the abundance of meltwater reaching the glacier bed (ibid.). In order to retain V-type valley shape as found in this study, the glaciers should have had very limited basal meltwater and temperate ice during the LIA and prior, despite of thicker ice in that times. The ice thickness may have played limited impact on erosion if no meltwater reached glacier bed as observed by Koppes et al. (2015) in Antarctica.

We found high scattering facies near the frontal margins of the studied glaciers, which we relate to incorporated debris in the basal ice (see reasoning in Results). An alternative interpretation of the scattering zones may be related to temperate ice as it was done, for example, by Rippin et al. (2011) who found temperate ice near the snout of the Kårsaglaciären, northern Sweden, throughout the entire ice thickness, which was less than 50 m. They interpreted the temperate ice as remnant of past glacier geometry and climate. Gillespie et al. (2023) also found temperate ice Lyngmarksbræen Ice Cap, West Greenland, in place only 15 m from the surface but interpreted its origin to be connected to cryo-hydrological warming from water percolation and freezing in crevasses. In our case, there are no open crevasses and no snow or firn for surface meltwater to freeze inside, thus we can reject the latter idea. It also seems unlikely that the thickness of possible temperate ice would increase towards the glacier's margins where ice becomes thinner as we would expect the diminishing temperate ice layer due to increased heat losses and also loss of temperate ice due to winter cold wave, as winters at this location are especially long and cold (the mean temperature in winter months is typically lower than -20 °C at the sea level (Sugiyama et al., 2014)). Thus, in our case, we do not support the idea that intense scattering would be related to temperate ice at all, even as a remnant.

Debris in the basal ice may suggest that some bed erosion has occurred in places, and glaciers were polythermal during the LIA maximum, although the preservation of V-shaped subglacial valleys does not support an idea of widespread erosion and distribution of temperate ice. Also, it is not clear how exactly the presence of debris inside the ice is connected to the erosion of glacial valleys as they seem to be modified only slightly. Debris may be a result of mass movements on valley slopes prior the glacier advance in these parts of the valleys, which may have occurred before the LIA when the glacier extent was smaller (Søndergaarde et., 2019). They may possibly be generated due to the glacier advance over talus material that may be expected in the case of such steep and narrow valleys as was suggested for small glaciers in Svalbard by King et al. (2008) and it does not require subglacial erosion at all. Limited subglacial erosion and cold-based ice was noted also from the studies of cosmogenic isotope inheritance problems in boulders near Thule (Corbett et al., 2014). A volume of debris inside the glacier also do not have to be large to create intense GPR signal scattering it may be limited to a rock fraction below 10% and even 2.5% (Santin et al., 2023). Alternatively, the debris material may be generated at higher elevations beneath the ice cap and outside the narrow valley. Further clast shape and grain surface characteristics and microtexture analyses may be advised to infer sediment transport paths and glacial influence as has been done elsewhere in Svalbard and Greenland (e.g. Kalińska-Nartiša et al., 2017a; 2017b; Evans et al., 2022) but was out of scope of this study.

A common assumption is that glacial erosion develops U-shaped valleys (also catenary curve that can be approximated by parabolas) from initially V-shaped fluvial valleys due to their widening and deepening (Hirano & Aniya, 1988; Harbor, 1992) as is nowadays demonstrated by quantitative analyses (e.g. Prasicek et al., 2015) and modelling (e.g. Brædstrup et al., 2016). However, Montgomery (2002) found that if the glacier drainage areas are smaller than 10 km^2, the differences of cross-sectional areas of glaciated valleys and fluvial valleys may be small or non-existent. Also Zimmer & Gabet (2018) found that V- and U-shaped valleys are present in both glaciated and non-glaciated terrains. Findings from North America show even more interesting valley profiles where narrow V-shaped preglacial fluvial gorges and valleys are buried within U-shaped glacial valleys (Lajeunesse, 2014). Specific topography and most likely cold-based stagnant ice masses with no, or limited, basal meltwater should be necessary to preserve such valleys. Our data demonstrates that small, glaciated valleys in NW Greenland retain V-shaped cross-section, despite of still sustaining valley glaciers, which have even been suggested to be warm-based during the Little Ice Age (Carrivick et al., 2023). Our finding of V-shaped subglacial valleys in cold polar settings may be further explained by largely cold-based nature of small outlet glaciers not only in today but in the past as well. Similar conclusions were drawn by Bælum & Benn (2011) from studies on Tellbreen, Svalbard. Thus, the mentioned examples and this study suggests more widespread phenomenon of V-shaped glacial valleys.

6. CONCLUSIONS

We have presented the GPR surveys of the Qaanaaq and neighbouring glacier in NW Greenland complemented with UAV surveys. We reveal up to 170-m-thick and completely cold ice filling narrow V-shaped subglacial valleys. We demonstrate that the assumption of 80 m to 100 m ice thickness as a threshold of Arctic glaciers needed to sustain temperate ice (Murray et al., 2000; Carrivick et al., 2023) is not applicable for glaciers at high latitudes in Greenland, which may be completely cold, although reaching much higher ice thickness. We suggest that the dynamics, distribution of temperate ice and subglacial erosion of the studied glaciers should have been limited also during the Last Ice Age to sustain the survival of the V-shaped glacial valleys. Thus, the classical transformation of V-shaped fluvial valleys into the U-shaped glacial valleys may be restricted beneath such small High Arctic glaciers under specific conditions of glacier geometry, subglacial topography, thermal regime and glaciation history among other potential factors.

The comparison of the ice thickness model of Millan et al. (2022) with our data reveals that, while the mean ice thickness may differ a little, the thickness is greatly underestimated in modelled data along the central axis of the subglacial valleys and overestimated near valley flanks suggesting a need for further improvements in ice thickness modelling for small and narrow glaciers.

This study allows us to accentuate the significance of in-situ glaciological measurements of the peripheral glaciers in Greenland due to their highly variable geometries, thermal structure, glaciation history and related regional and local climatic, geological, topographic and many other factors.

ACKNOWLEDGEMENTS

This work was supported by the performance-based funding (grant No. AAp2016/B041//Zd2016/AZ03) of the University of Latvia within the project "Climate change and sustainable use of natural resources". A part of the field activity was funded by Arctic Challenge for sustainability research project II (ArCS II: JPMXD1420318865).
INTERACT (**https://eu-interact.org/**) financially supported our access to DMI Qaanaaq. Arctic DEMs provided by the Polar Geospatial Center under NSF-OPP awards 1043681, 1559691, 1542736, 1810976, and 2129685.

AUTHOR CONTRIBUTIONS

Conceptualization: Kristaps Lamsters and Jānis Karušs. Methodology: all authors. GPR survey and processing: Jānis Karušs, Jurijs Ješkins and Pēteris Džeriņš. UAV survey and processing: Shinta Ukai and Shin Sugiyama. GIS analyses and map production: Kristaps Lamsters. Writing, first draft: Kristaps Lamsters and Jānis Karušs. Writing, review and editing: Kristaps Lamsters, Jānis Karušs and Shin Sugiyama. All authors read and approved the final manuscript.

CONFLICT OF INTEREST STATEMENT

The authors declare that they have no known competing financial interests or personal relationships that could have appeared to influence the work reported in this paper.

DATA AVAILABILITY STATEMENT

Data are available upon request from the corresponding author.

References

Alley, R.B., Cuffey, K.M. & Zoet, L.K. (2019) Glacial erosion: status and outlook. Annals of Glaciology, 60(80), 1–13. https://doi.org/10.1017/aog.2019.38

Bælum, K. & Benn, D.I. (2011) Thermal structure and drainage system of a small valley glacier (Tellbreen, Svalbard), investigated by ground penetrating radar. The Cryosphere, 5(1), 139–149. https://doi.org/10.5194/tc-5-139-2011

Barrett, B.E., Murray, T. & Clark, R. (2007) Errors in radar CMP velocity estimates due to survey geometry, and their implication for ice water content estimation. Journal of Environmental and Engineering Geophysics, 12(1), 101–111. https://doi.org/10.2113/JEEG12.1.101

Björnsson, H., Gjessing, Y., Hamran, S.E., Hagen, J.O., LiestøL, O., Pálsson, F. & Erlingsson, B. (1996) The thermal regime of sub-polar glaciers mapped by multi-frequency radio-echo sounding. Journal of Glaciology, 42(140), 23–32. https://doi.org/10.3189/S0022143000030495

Bolch, T., Sandberg Sørensen, L., Simonsen, S.B., Mölg, N., Machguth, H., Rastner, P. & Paul, F. (2013). Mass loss of Greenland's glaciers and ice caps 2003–2008 revealed from ICESat laser altimetry data. Geophysical Research Letters, 40(5), 875–881. https://doi.org/10.1002/grl.50270

Bradford, J.H. & Harper, J.T. (2005) Wave field migration as a tool for estimating spatially continuous radar velocity and water content in glaciers. Geophysical Research Letters, 32, L08502. https://doi.org/10.1029/2004GL021770

Brædstrup, C.F., Egholm, D.L., Ugelvig, S.V. & Pedersen, V.K. (2016) Basal shear stress under alpine glaciers: insights from experiments using the iSOSIA and Elmer/Ice models. Earth Surface Dynamics, 4(1), 159–174. https://doi.org/10.5194/esurf-4-159-2016

Bull, W.B. & McFadden, L. (1977) Tectonic geomorphology North and South of the Garlock fault, California. In: Dohring, D.O. (Ed.),

Geomorphology in Arid Regions. State University of New York, Binghamton, pp. 115–138.
Carrivick, J.L., Smith, M.W., Sutherland, J.L. & Grimes, M. (2023) Cooling glaciers in a warming climate since the Little Ice Age at Qaanaaq, northwest Kalaallit Nunaat (Greenland). Earth Surface Processes and Landforms, 48(13), 2446–2462. https://doi.org/10.1002/esp.5638
Corbett, L.B., Bierman, P.R., Lasher, G.E. & Rood D.H. (2014) Landscape chronology and glacial history in Thule, northwest Greenland. Quaternary Science Reviews, 109, 57–67. https://doi.org/10.1016/j.quascirev.2014.11.019
Daxberger, H., Dalumpines, R., Scott, D.M. & Riller, U. (2014) The ValleyMorph Tool: An automated extraction tool for transverse topographic symmetry (T-) factor and valley width to valley height (Vf-) ratio. Computers & Geosciences, 70, 154–163. https://doi.org/10.1016/j.cageo.2014.05.015
Evans, D.J., Ewertowski, M., Roberts, D.H. & Tomczyk, A.M. (2022) The historical emergence of a geometric and sinuous ridge network at the Hørbyebreen polythermal glacier snout, Svalbard and its use in the interpretation of ancient glacial landforms. Geomorphology, 406, 108213. https://doi.org/10.1016/j.geomorph.2022.108213
Ewertowski, M.W., Evans, D.J., Roberts, D.H., Tomczyk, A.M., Ewertowski, W. & Pleksot, K. (2019a) Quantification of historical landscape change on the foreland of a receding polythermal glacier, Hørbyebreen, Svalbard. Geomorphology, 325, 40–54. https://doi.org/10.1016/j.geomorph.2018.09.027
Ewertowski, M.W.; Tomczyk, A.M.; Evans, D.J.A.; Roberts, D.H. & Ewertowski, W. (2019b) Operational Framework for Rapid, Very-high Resolution Mapping of Glacial Geomorphology Using Low-cost Unmanned Aerial Vehicles and Structure-from-Motion Approach. Remote Sensing 11(1), 65. https://doi.org/10.3390/rs11010065
Farinotti, D., King, E.C., Albrecht, A., Huss, M. & Gudmundsson, G.H. (2014) The bedrock topography of Starbuck Glacier, Antarctic

Peninsula, as determined by radio-echo soundings and flow modeling. Annals of Glaciology, 55(67), 22–28. https://doi.org/10.3189/2014AoG67A025

Farinotti, D., Brinkerhoff, D.J., Clarke, G.K., Fürst, J.J., Frey, H., Gantayat, P., Gillet-Chaulet, F., Girard, C., Huss, M., Leclercq, P.W. & Linsbauer, A. (2017) How accurate are estimates of glacier ice thickness? Results from ITMIX, the Ice Thickness Models Intercomparison eXperiment. The Cryosphere, 11(2), 949–970. https://doi.org/10.5194/tc-11-949-2017

Farinotti, D., Huss, M., Fürst, J.J., Landmann, J., Machguth, H., Maussion, F. & Pandit, A. (2019) A consensus estimate for the ice thickness distribution of all glaciers on Earth. Nature Geoscience, 12, 168–173. https://doi.org/10.1038/s41561-019-0300-3

Forte, E., Santin, I., Ponti, S., Colucci, R.R., Gutgesell, P. & Guglielmin, M. (2021) New insights in glaciers characterization by differential diagnosis integrating GPR and remote sensing techniques: A case study for the Eastern Gran Zebrù glacier (Central Alps). Remote Sensing of Environment, 267, 112715. https://doi.org/10.1016/j.rse.2021.112715

Gillespie, M.K., Yde, J.C., Andresen, M.S., Citterio, M. & Gillespie, M.A.K. (2023) Ice geometry and thermal regime of Lyngmarksbræen Ice Cap, West Greenland. Journal of Glaciology, 1–13. https://doi.org/10.1017/jog.2023.89

Gusmeroli, A., Murray, T., Jansson, P., Pettersson, R., Aschwanden, A. & Booth, A.D. (2010) Vertical distribution of water within the polythermal Storglaciären, Sweden. Journal of Geophysical Research: Earth Surface, 115, F04002. https://doi.org/10.1029/2009JF001539

Hagen, J.O., Liestøl ,O., Roland, E. & Jørgensen, T. (1993). Glacier Atlas of Svalbard. Oslo: Norsk Polarinstitut.

Hall, A.M., Ebert, K., Kleman, J., Nesje, A. & Ottesen, D. (2013) Selective glacial erosion on the Norwegian passive margin. Geology, 41(12), 1203–1206. https://doi.org/10.1130/G34806.1

Hallet, B., Hunter, L. & Bogen, J. (1996) Rates of erosion and sediment yield by glaciers: A review of field data and their implications. Global and Planetary Change, 12, 213–235. https://doi.org/10.1016/0921-8181(95)00021-6

Harbor, J.M. (1992) Numerical modeling of the development of U-shaped valleys by glacial erosion. Geological Society of America Bulletin, 104, 1364–1375. https://doi.org/10.1130/0016-7606(1992)104<1364:NMOTDO>2.3.CO;2

Henriksen, N., Higgins, A.K., Kalsbeek, F. & Pulvertaft, T.C.R. (2009) Greenland from Archean to Quaternary: Descriptive text to the 1995 geological map of Greenland, 1:2 500 000. Geological Survey of Denmark and Greenland Bulletin 18.

Hirano, M. & Aniya, M. (1988) A rational explanation of cross-profile morphology for glacial valleys and of glacial valley development. Earth Surface Processes and Landforms, 13, 707–716. https://doi.org/10.1002/esp.3290130805

Hock, R., Bliss, A., Marzeion, B., Giesen, R.H., Hirabayashi, Y., Huss, M., Radić, V. & Slangen, A.B.A. (2019) GlacierMIP – A model intercomparison of global-scale glacier mass-balance models and projections. Journal of Glaciology, 65, 453–467. https://doi.org/10.1017/jog.2019.22

Hock, R., Maussion, F., Marzeion, B. & Nowicki, S. (2023) What is the global glacier ice volume outside the ice sheets? Journal of Glaciology, 69, 204–210. https://doi.org/10.1017/jog.2023.1

IPCC: Summary for Policymakers. (2021) In: Climate Change 2021: The Physical Science Basis. Contribution of Working Group I to the Sixth Assessment Report of the Intergovernmental Panel on Climate Change, edited by: Masson-Delmotte, V., Zhai, P., Pirani, A., Connors, S. L., Péan, C., Berger, S., Caud, N., Chen, Y., Goldfarb, L., Gomis, M. I., Huang, M., Leitzell, K., Lonnoy, E., Matthews, J. B. R., Maycock, T. K., Waterfield, T., Yelekçi, O., Yu, R., & Zhou, B., Cambridge University Press, Cambridge, United Kingdom and New York, NY, USA, 3–32.

Irvine-Fynn, T.D., Hodson, A.J., Moorman, B.J., Vatne, G. & Hubbard, A.L. (2011) Polythermal glacier hydrology: A review. Reviews of Geophysics, 49(4), RG4002. https://doi.org/10.1029/2010RG000350

Jacob, R.W. & Hermance, J.F. (2004) Assessing the precision of GPR velocity and vertical two-way travel time estimates. Journal of Environmental and Engineering Geophysics, 9(3), 143–153. https://doi.org/10.4133/JEEG9.3.143

Jansen, J.D., Knudsen, M.F., Andersen, J.L., Heyman, J. & Egholm, D.L. (2019) Erosion rates in Fennoscandia during the past million years. Quaternary Science Reviews, 207, 37–48. https://doi.org/10.1016/j.quascirev.2019.01.010

Kalinska-Nartiša, E., Lamsters, K., Karušs, J., Krievāns, M., Rečs, A. & Meija, R. (2017a) Quartz grain features in modern glacial and proglacial environments: A microscopic study from the Russell Glacier, southwest Greenland. Polish Polar Research, 38(3), 265–289. DOI: 10.1515/popore-2017-0018

Nartiša, E.K., Lamsters, K., Karušs, J., Krievāns, M., Rečs, A. & Meija, R. (2017b) Fine-grained quartz from cryoconite holes of the Russell Glacier, southwest Greenland–a scanning electron microscopy study. Baltica, 30(2), 63–73. http://dx.doi.org/10.5200/baltica.2017.30.08

Karušs, J., Lamsters, K., Sobota, I., Ješkins, J. & Džeriŋš, P. (2022a) UAV and GPR Data Integration in Glacier Geometry Reconstruction: A Case Study from Irenebreen, Svalbard. Remote Sensing 14 (3), 456. https://doi.org/10.3390/rs14030456

Karušs, J., Lamsters, K., Sobota, I., Ješkins, J., Džeriŋš, P. & Hodson, A. (2022b). Drainage system and thermal structure of a High Arctic polythermal glacier: Waldemarbreen, western Svalbard. Journal of Glaciology, 68 (269), 591–604. https://doi.org/10.1017/jog.2021.125

Karušs, J., Lamsters, K., Chernov, A., Krievāns, M. & Ješkins, J. (2019) Subglacial topography and thickness of ice caps on the Argentine

Islands. Antarctic Science, 31, 332–344. https://doi.org/10.1017/S0954102019000452

Karušs, J., Lamsters, K., Poršņovs, D., Zandersons, V. & Ješkins, J. (2021) Geophysical mapping of residual pollution at the remediated Inčukalns acid tar lagoon, Latvia. Estonian Journal of Earth Sciences, 70(3), 140–151. https://doi.org/10.3176/earth.2021.10

Khan, S.A., Colgan, W., Neumann, T.A., Van Den Broeke, M.R., Brunt, K.M., Noël, B., Bamber, J.L., Hassan, J. & Bjørk, A.A. (2022) Accelerating ice loss from peripheral glaciers in North Greenland. Geophysical Research Letters, 49(12), e2022GL098915. https://doi.org/10.1029/2022GL098915

King, E.C., Smith, A.M., Murray, T. & Stuart, G.W. (2008) Glacier-bed characteristics of Midtre Lovénbreen, Svalbard, from high-resolution seismic and radar surveying. Journal of Glaciology, 54(184), 145–156. https://doi.org/10.3189/002214308784409099

Kleman, J. & Hättestrand, C. (1999) Frozen-bed Fennoscandian and Laurentide ice sheets during the Last Glacial Maximum. Nature, 402(6757), 63–66. https://doi.org/10.1038/47005

Kondo, K., Sugiyama, S., Sakakibara, D. and Fukumoto, S. (2021) Flood events caused by discharge from QG, northwestern Greenland. Journal of Glaciology, 67(263), 500–510. https://doi.org/10.1017/jog.2021.3

Koppes, M., Hallet, B., Rignot, E., Mouginot, J., Wellner, J.S. & Boldt, K. (2015). Observed latitudinal variations in erosion as a function of glacier dynamics. Nature, 526(7571),100–103. https://doi.org/10.1038/nature15385

Lajeunesse, P. (2014). Buried preglacial fluvial gorges and valleys preserved through Quaternary glaciations beneath the eastern Laurentide Ice Sheet. GSA Bulletin, 126(3-4), 447–458. https://doi.org/10.1130/B30911.1

Lamsters, K., Karušs, J., Krievāns, M. & Ješkins, J. (2020a). High-Resolution Surface and Bed Topography Mapping of Russell Glacier (SW Greenland) Using UAV and GPR. ISPRS Annals of the

Photogrammetry, Remote Sensing and Spatial Information Sciences, 2, 757–763. https://doi.org/10.5194/isprs-annals-V-2-2020-757-2020

Lamsters, K., Karušs, J., Krievāns, M. & Ješkins, J. (2020b) The thermal structure, subglacial topography and surface structures of the NE outlet of Eyjabakkajökull, east Iceland. Polar Science, 26, 100566. https://doi.org/10.1016/j.polar.2020.100566

Lamsters, K., Ješkins, J., Sobota, I., Karušs, J. & Džeriņš, P. (2022) Surface Characteristics, Elevation Change, and Velocity of High-Arctic Valley Glacier from Repeated High-Resolution UAV Photogrammetry. Remote Sensing, 14(4), 1029. https://doi.org/10.3390/rs14041029

Larocca, L.J., Twining–Ward, M., Axford, Y., Schweinsberg, A.D., Larsen, S.H., Westergaard–Nielsen, A., Luetzenburg, G., Briner, J.P., Kjeldsen, K.K. & Bjørk, A.A. (2023) Greenland-wide accelerated retreat of peripheral glaciers in the twenty-first century. Nature Climate Change, 13, 1324–1328. https://doi.org/10.1038/s41558-023-01855-6

Leith, K., Moore, J.R., Amann, F. & Loew, S. (2014) Subglacial extensional fracture development and implications for Alpine Valley evolution. Journal of Geophysical Research: Earth Surface, 119(1), 62–81. https://doi.org/10.1002/2012JF002691

Leng, Z. & Al-Qadi, I.L. An innovative method for measuring pavement dielectric constant using the extended CMP method with two air-coupled GPR systems. NDT&E International 2014, 66, 90–98. https://doi.org/10.1016/j.ndteint.2014.05.002

Lidmar-Bergström, K. (1997) A long-term perspective on glacial erosion. Earth Surface Processes and Landforms: The Journal of the British Geomorphological Group, 22(3), 297–306.

Macheret, Yu.Ya., Moskalevsky, M.Yu. & Vasilenko, E.V. (1993) Velocity of radio waves in glaciers as an indicator of their hydrothermal state, structure and regime. Journal of Glaciology, 39(132), 373–384. https://doi.org/10.3189/S0022143000016038

Millan, R., Mouginot, J., Rabatel, A., Morlighem, M. (2022). Ice velocity and thickness of the world's glaciers. Nature Geoscience, 15(2), 124–129. https://doi.org/10.1038/s41561-021-00885-z

Montgomery, D.R. (2002) Valley formation by fluvial and glacial erosion. Geology, 30(11), 1047–1050. https://doi.org/10.1130/0091-7613(2002)030<1047:VFBFAG>2.0.CO;2

Murray, T. Stuart, G.W., Miller, P.J., Woodward, J., Smith, A.M., Porter, P.R. & Jiskoot, H. (2000) Glacier surge propagation by thermal evolution at the bed. Journal Geophysical Research: Solid Earth, 105(B6), 13491–13507. https://doi.org/10.1029/2000JB900066

Navarro, F. & Eisen, O. (2009) Ground-penetrating radar in glaciological applications. In: Pellikka, P., Rees, W.G. (Eds.) Remote Sensing of Glaciers. Techniques for Topographic, Spatial and Thematic Mapping of Glaciers. Taylor & Francis Group, London, UK, pp. 195–231.

Nghiem, S.V., Hall, D.K., Mote, T.L., Tedesco, M., Albert, M.R., Keegan, K., Shuman, C.A., DiGirolamo, N.E. & Neumann, G. (2012) The extreme melt across the Greenland ice sheet in 2012. Geophysical Research Letters, 39(20). https://doi.org/10.1029/2012GL053611

Patton, H., Hubbard, A., Heyman, J., Alexandropoulou, N., Lasabuda, A.P., Stroeven, A.P., Hall, A.M., Winsborrow, M., Sugden, D.E., Kleman, J. & Andreassen, K. (2022) The extreme yet transient nature of glacial erosion. Nature Communications, 13(1), 7377. https://doi.org/10.1038/s41467-022-35072-0

Pettersson, R., Jansson, P., & Holmlund, P. 2003. Cold surface layer thinning on Storglaciären, Sweden, observed by repeated ground penetrating radar surveys. Journal of Geophysical Research, 108(F1), 6004–6005. https://doi.org/10.1029/2003JF000024

Porter, C., Howat, I., Noh, M.J., Husby, E., Khuvis, S., Danish, E., Tomko, K., Gardiner, J., Negrete, A., Yadav, B., Klassen, J., Kelleher, C., Cloutier, M., Bakker, J., Enos, J., Arnold, G., Bauer, G. & Morin, P., 2023, "ArcticDEM – Strips, Version 4.1", Available from: https://doi.org/10.7910/DVN/3VDC4W, Harvard Dataverse, V1.

Prasicek, G., Otto, J.C., Montgomery, D.R. & Schrott, L. (2015) Glaciated valleys in Europe and western Asia. Journal of Maps, 11(2), 361–370. https://doi.org/10.1080/17445647.2014.921647

Precise Point Positioning. (n.d.). Canadian Spatial Reference System Precise Point Positioning (CSRS-PPP). Natural Resources Canada. Available at: https://webapp.csrs-scrs.nrcan-rncan.gc.ca/geod/tools-outils/ppp.php

Rippin, D.M., Carrivick, J.L. & Williams, C. (2011) Evidence towards a thermal lag in the response of Kårsaglaciären, northern Sweden, to climate change. Journal of Glaciology, 57(205), 895–903. https://doi.org/10.3189/002214311798043672

Saito, J., Sugiyama, S., Tsutaki, S., Sawagaki, T. (2016) Surface elevation change on ice caps in the Qaanaaq region northwestern Greenland. Polar Science, 10, 239–248. https://doi.org/10.1016/j.polar.2016.05.002

Santin, I., Roncoroni, G., Forte, E., Gutgesell, P. & Pipan, M. (2023) GPR modelling and inversion to quantify the debris content within ice. Near Surface Geophysics, 1–15. https://doi.org/10.1002/nsg.12274

Sevestre, H., Benn D.I., Hulton N.R. & Bælum, K. (2015) Thermal structure of Svalbard glaciers and implications for thermal switch models of glacier surging. Journal of Geophysical Research: Earth Surface 120(10), 2220–2236. https://doi.org/10.1002/2015JF003517

Søndergaard, A.S., Larsen, N.K., Olsen, J., Strunk, A. & Woodroffe, S. (2019) Glacial history of the Greenland Ice Sheet and a local ice cap in Qaanaaq, northwest Greenland. Journal of Quaternary Science, 34(7), 536–547. https://doi.org/10.1002/jqs.3139

Sugiyama, S. (2020) Through the Japanese field research in Greenland: A changing natural environment and its impact on human society. Polar Record, 56, e8. https://doi.org/10.1017/S003224742000011X

Sugiyama, S., Kanna, N., Sakakibara, D., Ando, T., Asaji, I., Kondo, K., Wang, Y., Fujishi, Y., Fukumoto, S., Podolskiy, E. & Fukamachi, Y. (2021) Rapidly changing glaciers, ocean and coastal environments, and their impact on human society in the Qaanaaq region, northwestern Greenland. Polar Science, 27, 100632. https://doi.org/10.1016/j.polar.2020.100632

Sugiyama, S., Sakakibara, D., Matsuno, S., Yamaguchi, S., Matoba, S. & Aoki, T. (2014) Initial field observations on Qaanaaq ice cap, Northwestern Greenland. Annals of Glaciology, 55(66), 25–33. https://doi.org/10.3189/2014AoG66A102

Tsutaki, S., Sugiyama, S., Sakakibara, D., Aoki, T. & Niwano, M. (2017) Surface mass balance, ice velocity and near-surface ice temperature on Qaanaaq ice cap, northwest Greenland, from 2012 to 2016. Annals of Glaciology, 58(75), 18–92. https://doi.org/10.1017/aog.2017.7

Van der Veen, C.J. & I.M. Whillans. (1989) Force budget: I. Theory and numerical methods. Journal of Glaciology, 35(119), 53–60.

Woodward, J., Murray, T., Clark, R.A. & Stuart, G.W. (2003) Glacier surge mechanisms inferred from ground-penetrating radar: Kongsvegen Svalbard. Journal Glaciology, 49(167), 473–480. https://doi.org/10.3189/172756503781830458

Yde, J.C., Gillespie, M.K., Løland, R., Ruud, H., Mernild, S.H., Villiers, S.D., Knudsen, N.T. & Malmros, J.K. (2014) Volume measurements of Mittivakkat Gletscher, southeast Greenland. Journal of Glaciology, 60(224), 1199–1207. https://doi.org/10.3189/2014JoG14J047

Zimmer, P.D. & Gabet, E.J. (2018) Assessing glacial modification of bedrock valleys using a novel approach. Geomorphology, 318, 336–347. https://doi.org/10.1016/j.geomorph.2018.06.021